Structure/Property Relations in Bulk Versus Solution Derived Proton Conducting Ceramics of the Form $SrCe_{0.95}Yb_{0.05}O_{3-\delta}$ With Applications in Membrane Separations

Kyle S. Brinkman[1] Elise B. Fox[1], Paul Korinko[1], Rob Lascola[1], Frank Chen[2]
[1]Materials Science and Technology Directorate, Savannah River National Laboratory (SRNL)
Aiken, SC 29808, U.S.A.
[2]Department of Mechanical Engineering, University of South Carolina,
Columbia, SC 20208, USA

ABSTRACT

Membrane separations are a key enabling technology for future energy conversion devices. Ionic transport membranes must have both proton and electronic conductivity to function as hydrogen separation membranes without an external power supply. A technical obstacle to material modification by compositional changes is that the hydrogen flux through a dense membrane is a function of both the proton ionic conductivity and the electronic conductivity. An alternative way to modify the materials conductivity without changing the ratio of the chemical constituents is by altering the microstructure. In this study, $SrCe_{0.95}Yb_{0.05}O_3$ was produced by conventional mixed oxide bulk ceramic techniques and chemical solution routes self-rising approaches using urea as the leavening agent. In conventional ceramic processing routes, the perovskite phase was observed to form at temperatures near 1300°C, while solution techniques resulted in perovskite phase formation starting near 1000°C with complete phase transformations occurring at 1100°C. Thermogravimetric analysis (TGA) was conducted in various gas atmospheres resulting in bulk oxide route powders exhibiting a 0.6% weight loss at 800°C under a nitrogen environment as compared to chemically derived powders which displayed weight losses on the order of 3.4%.The increase weight loss observed in chemically derived $SrCe_{0.95}Yb_{0.05}O_3$ is correlated with an increase in the number of electron charge carriers and results in elevated electronic conduction. This study will report on the development structure property relations in the model proton conducting ceramic system $SrCe_{0.95}Yb_{0.05}O_3$.

INTRODUCTION

Membrane separations are a key enabling technology for future energy conversion devices[1]. Ionic transport membranes must have both proton and electronic conductivity to function as hydrogen separation membranes without an external power supply. In addition, the materials electronic conductivity or material crystal structure stability should not be greatly affected by the presence of contaminant gases (CO_2, CO, CH_4 and H_2O from steam reforming/water gas shift reactions). Perovskite materials of the general formula $SrCeO_3$ and $BaCeO_3$ form the basis of most ceramic compositions with proton conductivities in the range of 2 X 10^{-2} S/cm at 600°C, showing good stability under the extremely low oxygen partial pressure where many perovskites decompose to their primary oxides[2]. “A”-site doping of the ABO_3 perovskite structure and stoichiometry modifications have been explored to increase the stability under contaminated gases while maintaining acceptable proton conductivity levels, however the applications of these materials to hydrogen separation membranes has not yet been explored to a large extent. Structure/property relations regarding the impact of microstructure on the hydrogen

flux through a dense membrane are of particular interest[3]. This work focuses on the synthesis and characterization of dense nanocrystalline $SrCe_{0.95}Yb_{0.05}O_3$ proton conducting ceramic membranes as a response to the demand for novel materials and the examination of fundamental structure/property relations in a model material system. Wet chemical techniques have been used to fabricate nanocrystalline ceramic materials which enable lower temperature densification and results in membranes with dramatically smaller grain size than that is obtainable with conventional solid-state reaction processing

EXPERIMENT

$SrCe_{0.95}Yb_{0.05}O_3$ was produced via self-rising approach using urea as the leavening agent and PVA as the dough former. $Sr(NO_3)_2$, $Ce(NO_3)_3{\cdot}6H_2O$ and $Yb(NO_3)_3{\cdot}6H_2O$ were mixed in stoichiometric ratio and dissolved into distilled water. Urea and PVA solution was added to the nitrate salt solution resulting in a sticky dough precursor upon solvent evaporation. The precursor was fired at 500°C to obtain an amorphous precursor powder and Thermogravimetric nalysis combined with Differential Scanning Calorimetry (TGA-DSC) was used to examine the precursor powder using a heating rate of 10°C per minute up to 1400°C. The gas flow was nominally kept at 50 sccm air equivalent 5oC/min on a x unit. Conventional bulk oxide processing was also employed by mixing $SrCO_3$, Yb_2O_3 and CeO_2 in the stoichiometric ratios followed by ball milling in ethanol and subsequent calcinations 1300°C 5 hours at 5°C/min followed by sintering at 1500°C for 10 hours at 2°C/min ramp rate. XRD was performed on a PanAnalytical X-ray diffractometer. The crystallite sizes were calculated by X-ray line broadening technique using Debye–Scherrer equation, $t = 0.9\gamma/\beta \cos \Theta$, where t is the particle size, γ the wavelength of radiation used (1.541 A °), β the line broadening of the peak or full-width at half maximum (FWHM; rad), and Θ is the angle of the diffraction peak. BET of the starting powders was performed on a Micromeritics ASAP 2010C. The fifteen point adsorption-desorption isotherms were collected at 77K. SEM and TEM electron microscope characterization was performed on FEI Quanta and XL 30 model system. Raman spectra were obtained with 532 nm excitation (Verdi-2W, Coherent, Inc.) in the backscattering mode, using an imaging probe (MultiRxn Probe, Kaiser Optical Systems) with a 5 mm working distance. Scattered light was detected with a holographic spectrometer (Holospec VPH, Kaiser Optical Systems) and CCD camera (DV420A, Andor) electrically cooled to -55 ^{o}C.

RESULTS AND DISCUSSION

The thermal process of as-synthesized $SrCe_{0.95}Yb_{0.05}O_3$ obtained by self-rising approach was recorded by TG/DSC is shown in Fig 1a. A continuous weight loss event was observed starting near 800°C which extends to 1000°C concomitant with an exothermic calorimetric signal near 1000°C indicating a crystallization event. To investigate the phase evolution, the as-synthesized $SrCe_{0.95}Yb_{0.05}O_3$ powders were calcined at temperatures from 600-1100°C in air for 5h. Fig 1b displays the XRD spectra of powders calcined at 500 and 1000ºC representing the amorphous starting material and initial $SrCe_{0.95}Yb_{0.05}O_3$ crystallization. As shown in Fig. 1b, the perovskite phase $SrCe_{0.95}Yb_{0.05}O_3$ was observed to form after calcination at 1000°C. Electron microscopy

(SEM/TEM) investigations on the resulting powder $SrCe_{0.95}Yb_{0.05}O_3$ synthesized by a self-rising route showed the material to be porous after high temperature calcinations displayed in Fig 2a-c). The average particle size as observed by TEM investigations was 100 nm when the calcination temperature was 1000°C as shown in Fig. 2b. However, the particle size increased sharply to 1µm after firing at 1100°C for 5h (shown in Fig. 2c). A relatively high calcination temperature was necessary in order to obtain single phase $SrCe_{0.95}Yb_{0.05}O_3$ which led to extensive grain growth and the particle coarsening to sized on the order of micron. Thermal analysis results demonstrate that the $SrCe_{0.95}Yb_{0.05}O_3$ powder involves the following steps ytterbium carbonate decomposition (endothermic onset at 580°C, and weight loss), and strontium carbonate decomposition (endothermic onset at 900°C, and associated weight loss), exothermic crystallization with peak near 1000°C with no associated weight loss with the process reaching completion at 1100°C.:

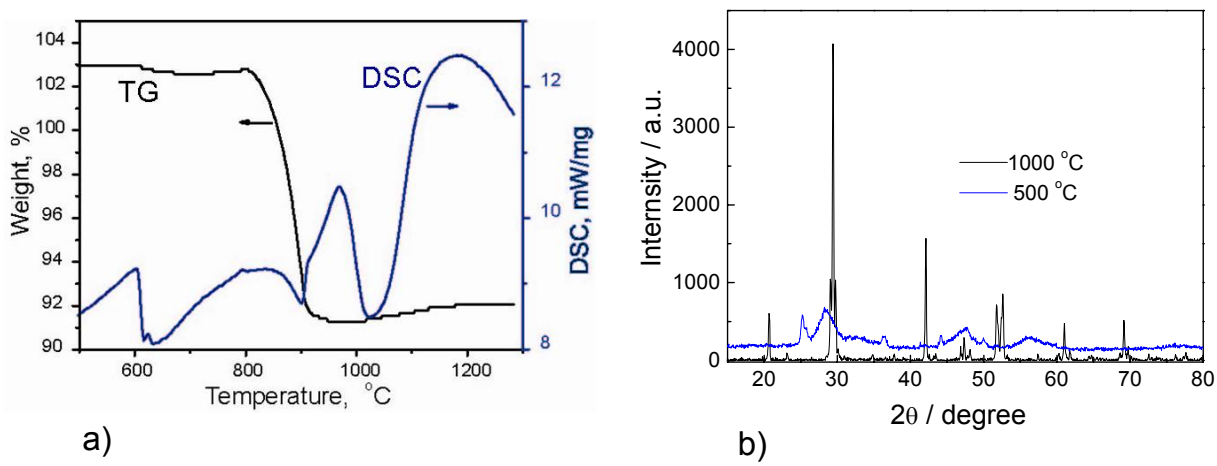

Figure 1 a) TG and DSC curves for the as-synthesized SrCe0.95Yb0.05O3 obtained by self-rising approach and b) XRD of $SrCe_{0.95}Yb_{0.05}O_3$ powders calcined at 500 and 1000 °C for 5h.

Fig. 3 displays the XRD and SEM results of $SrCe_{0.95}Yb_{0.05}O_3$ powders synthesized from the bulk oxide route calcined at 1300°C for 5 hours. Crystalline $SrCe_{0.95}Yb_{0.05}O_3$ was observed along with some residual CeO_2 precursor. Temperatures below 1300°C resulted in small amount of the target $SrCe_{0.95}Yb_{0.05}O_3$ phase. Table 1 presents the BET determined surface area of powders synthesized form the chemical and bulk oxide method in crystalline and amorphous forms with respective reaction temperatures. The traditional ball milling approach resulted in a low surface area mesoporous powder with a lower pore volume than the self-raising approach. The self-raising method produced a mesoporous powder with a higher surface area and pore volume that then the ball milling approach. As is seen in table , the chemical solution route employed in this study was successful in reducing the crystallization temperature from 1300°C in bulk oxide to 1100°C resulting in a reduced crystalline particle size from 10 micron (bulk oxide) to 1 micron (chemical route).

Table 1: Textural properties of $SrCe_{0.95}Yb_{0.05}O_3$ synthesized under various routes

	BET surface area m^2/g	Pore volume cm^3/g	Pore diameter nm	Crystallite size nm
$SrCe_{0.95}Yb_{0.05}O_3$ (ball milled)	2.2	0.003	19.8	
Amorphous $SrCe_{0.95}Yb_{0.05}O_3$ (self-rising)	63.9	0.081	8.6	

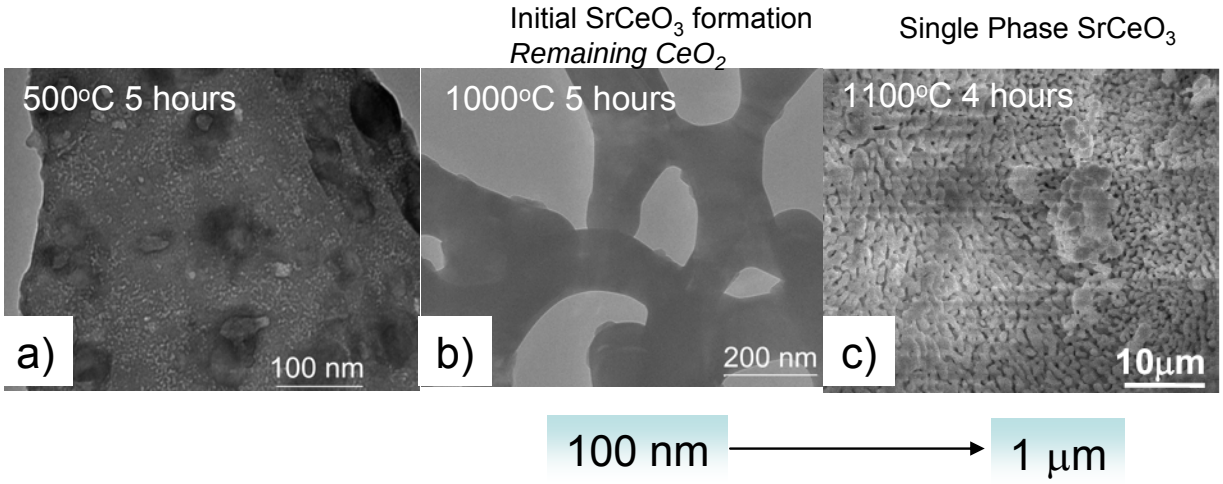

Figure 2 a) TEM of SrCeO3 after 500°C 5 hours, b) 1000°C 5 hours and c) SEM of particles after 1100°C for 5 hours.

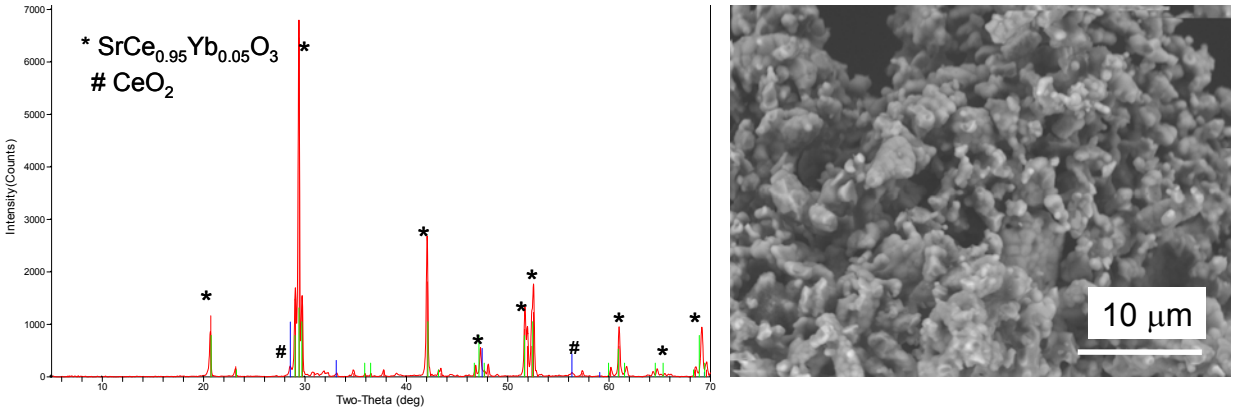

Figure 3 a) XRD and b) SEM bulk oxide powders at 1300°C 5 hours.

Figure 4. displays the SEM image ceramics sintered under the same conditions 1500°C at a 2°C/min ramp rate for 10 hours using starting powders obtained from the bulk oxide and self rising approach chemical solution route. Even at the elevated temperature of 1500°C for extended duration (10 hours), the initial size difference of the starting powders (1 micron solution, 10 micron bulk oxide) is reflected in the grain size of the sintered ceramics. The sintered ceramics via solution routes displayed a bi-modal grain size distribution from 1 to 8 microns, while the bulk oxide sintered ceramics showed grain sizes in excess of 12-15 microns.

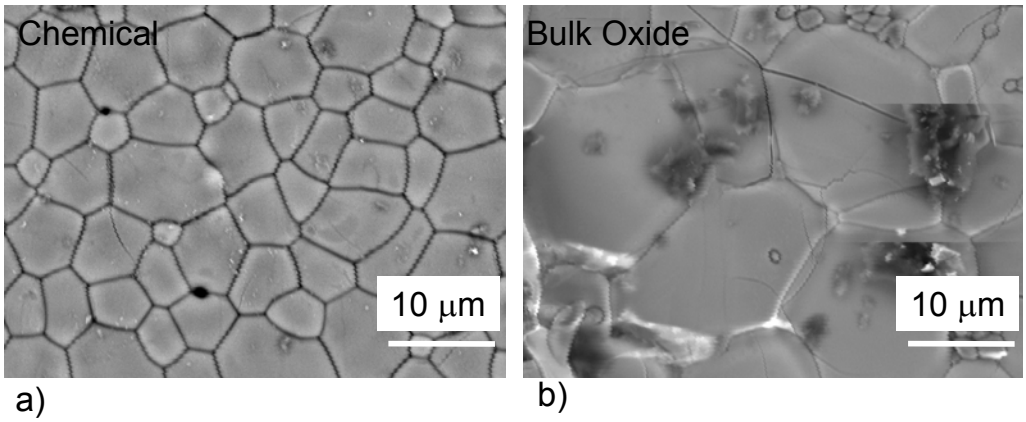

Figure 4 a) SEM of sintered chemical 1500°C and b) SEM of sintered ceramic bulk oxide 1500°C 10 hours

It is well known that the loss of oxygen from the lattice in these perovskite compounds results in positively charged oxygen "vacancies" which are compensated by electrons released from concomitant transition metal (Ce^{3+}/Ce^{4+}) reduction as described in equation (1)[2, 4]:

$$O_o^x \rightarrow V_O^{\bullet\bullet} + 2e' \quad \textit{and} \quad Ce^{4+} + e^- \leftrightarrow Ce^{3+} \textit{ or } 2\,CeO_2 \rightarrow Ce_2O_3 + 0.5\,O_2 \qquad (1)$$

Where $V_O^{\bullet\bullet}$ is a positively charged oxygen vacancy and e' is a negatively charged electron. In order to observe variations in oxygen non-stoichiometry in crystalline $SrCe_{0.95}Yb_{0.05}O_3$ powders synthesized from different methods TGA analysis was performed in both air and inert nitrogen gas environments. Figure 5 shows the weight loss data for the ceramic powders processed using these two processing routes. There is a significant difference in the weight loss and the increased weight loss observed in chemically derived $SrCe_{0.95}Yb_{0.05}O_3$ is correlated with an increase in the number of electron charge carriers and resulting in elevated electronic conduction in the material.

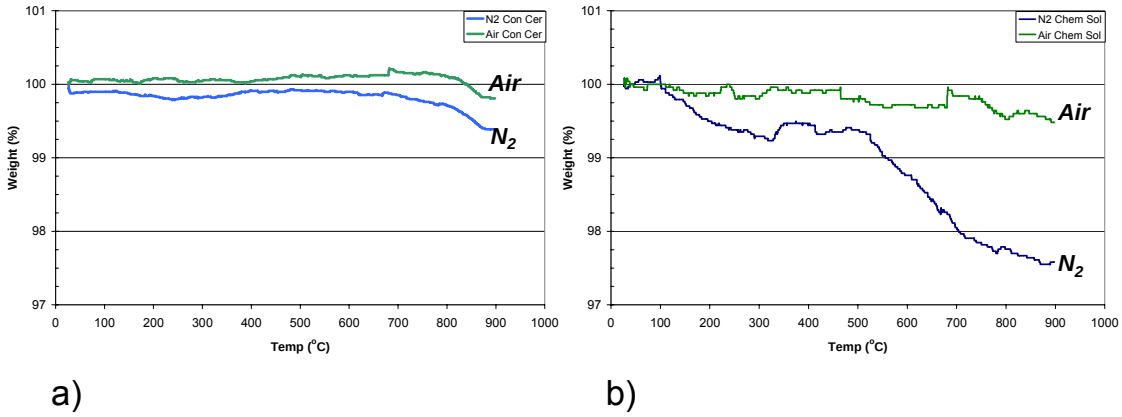

Figure 5 Thermogravimetric (TGA) studies of $SrCe_{0.95}Yb_{0.05}O_3$ prepared by a) bulk oxide route and b) chemical self-rising approach

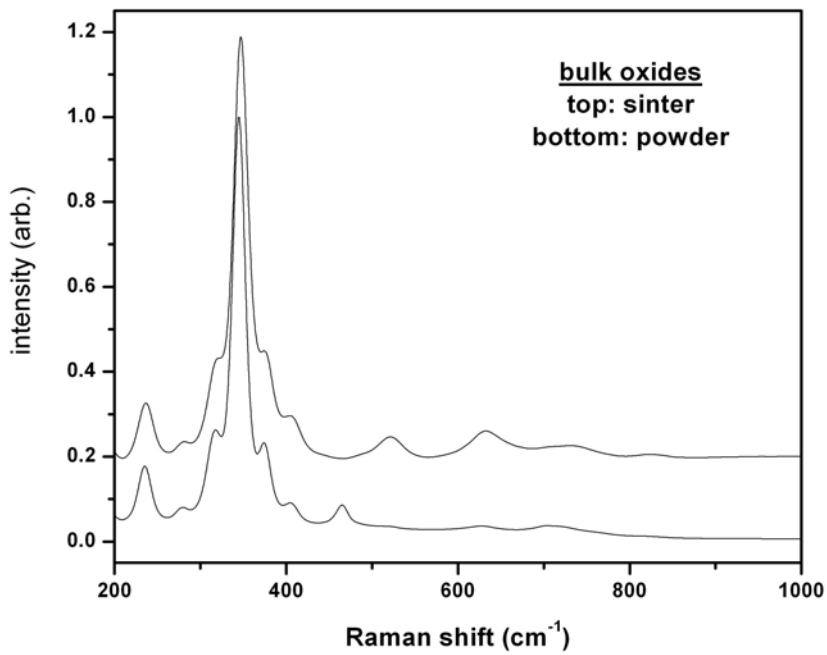

Figure 6 Raman spectra of crystalline $SrCe_{0.95}Yb_{0.05}O_3$ derived from bulk oxide powders and bulk oxide sintered ceramics.

Figure 6 displays the Raman spectra for crystalline $SrCe_{0.95}Yb_{0.05}O_3$ from bulk oxide powders and sintered ceramics. The spectrum is dominated by a band at ~365 cm^{-1} that is associated with vibrations of the CeO_6 octahedra in the crystal[5]. Peaks appearing at higher shifts are associated either with different material phases or with defects in the crystal. The peak at 460 cm^{-1} is associated with the fluorite-type structure of CeO_2 [6]. A preliminary interpretation suggests that the appearance of this peak is evidence of some kind of a phase separation in the material. It is not present in pure $SrCeO_3$ samples[7]. The peak at 630 cm^{-1} has been previously observed and

attributed to oxygen deficiencies in the doped lattice by Mineshige. The appearance of the band at 520 cm^{-1} may be associated with the 630 cm^{-1} band which is a feature shared with other systems, including $BaCeO_3$ and $Sr(Ce_{1-x}Zr_x)O_3$. This band (520 cm^{-1}) has not been examined in detail, but it may also be connected with oxygen vacancies.

CONCLUSIONS

Wet chemical techniques have been used to fabricate nanocrystalline ceramic membranes which enable lower temperature crystallization (1100°C) and result in dramatically smaller particle size (1 micron) than that is obtainable with conventional solid-state reaction processing (1300°C and 10 micron). Thermogravimetric (TGA) analysis showed that smaller, chemically derived powders exhibited near five times greater loss of oxygen (0.6% solid-state reaction, versus 3.4% chemical method) from the crystal lattice as compared to traditional oxide routes resulting in enhanced electronic conductivity. Oxygen non-stoichiometry was further examined using Raman spectroscopy to examine crystalline $SrCe_{0.95}Yb_{0.05}O_3$ from bulk oxide powders and sintered ceramics revealing bands associated with oxygen vacancies at630 cm^{-1}. Further experimental work is underway examining the conductivity determination versus processing and the viability of a reaction-sintering method aimed at achieving dense ceramic membranes to limit grain growth during sintering.

ACKNOWLEDGMENTS

This document was prepared in conjunction with work accomplished under Contract No. DE-AC09-08SR22470 with the U.S. Department of Energy. SRNL LDRD funding acknowledged for financial support.

REFERENCES

1. Phair, J.W. and S.P.S. Badwal, *Review of proton conductors for hydrogen separation.* Ionics, 2006. **12**(2): p. 103-115.
2. Iwahara, H., Esaka, T., Uchida, H. and Maeda, N, *Proton Conduction in Sintered Oxides and Its Application to Steam Electrolysis for Hydrogen-Production.* Solid State Ionics 1981. **3-4**: p. 159.
3. Song, S.J., Wachsman, E. D., Dorris, S. E. and Balachandran, U., *Defect structure and n-type electrical properties of SrCe0.95Eu0.05O3-d.* Journal of the Electrochemical Society, 2003. **150**: p. A1484.
4. Chiang, Y.M., et al., *Defect and transport properties of nanocrystalline CeO2-x.* Applied Physics Letters, 1996. **69**(2): p. 185-187.
5. Scherban, T., et al., *Raman-Scattering Study of Baceo3 and Srceo3.* Solid State Communications, 1992. **84**(3): p. 341-344.
6. Mineshige, A., et al., *Oxygen chemical potential variation in ceria-based solid oxide fuel cells determined by Raman spectroscopy.* Solid State Ionics, 2000. **135**(1-4): p. 481-485.
7. Loridant, S., G. Lucazeau, and T. Le Bihan, *A high-pressure Raman and X-ray diffraction study of the perovskite SrCeO3.* Journal of Physics and Chemistry of Solids, 2002. **63**(11): p. 1983-1992.